Development of impurity seeding and radiation enhancement in the helical divertor of LHD

Development of Impurity Seeding and Radiation Enhancement in the Helical Divertor of LHD

K. Mukai[1, 2], S. Masuzaki[1], B.J. Peterson[1, 2], T. Akiyama[1], M. Kobayashi[1, 2], H. Tanaka[1, 2], S.N. Pandya[3], R. Sano[1], G. Motojima[1], N. Ohno[4], T. Morisaki[1], C. Suzuki[1], I. Murakami[1], J. Miyazawa[1], N. Tamura[1], S. Yoshimura[1], I. Yamada[1], R. Yasuhara[1], H. Funaba[1], K. Tanaka[1] and the LHD Experiment Group[1]

[1]National Institute for Fusion Science, Toki, Gifu-ken 509-5292, Japan

[2]SOKENDAI (The Graduate University for Advanced Studies), Hayama 240-0163, Japan

[3]Institute for Plasma Research, Bhat, Gandhinagar 382 428, India

[4]Graduate School of Engineering, Nagoya Univ. Nagoya, Aichi-ken 464-8603, Japan

E-mail: mukai.kiyofumi@LHD.nifs.ac.jp

Abstract. Impurity seeding to reduce the divertor heat load was conducted in the Large Helical Device (LHD) using neon (Ne) and krypton (Kr) puffing. Radiation enhancement and reduction of the divertor heat load were observed. In the LHD, the ratio between the total radiated power and the heating power, $f_{rad} = P_{rad}/P_{heating}$, is limited up to around 30% in hydrogen plasmas even for high density plasma just below the radiative collapse ($n_{e,bar} > 1 \times 10^{20}$ m^{-3}), where $n_{e,bar}$ is the line averaged density. With Ne seeding, the ratio could be raised to 52% at $n_{e,bar} \sim 1.3 \times 10^{19}$ m^{-3}, albeit with a slight reduction in confinement. $f_{rad} \sim 30\%$ could be sustained for 3.4 s using multi-pulse Ne seeding at $n_{e,bar} \sim 4 \times 10^{19}$ m^{-3}. The localized supplemental radiation was observed along the helical divertor X-points (HDXs) which is similar to the estimated structure by the EMC3-EIRENE code. Kr seeding was also conducted at $n_{e,bar} \sim 3.1 \times 10^{19}$ m^{-3}. $f_{rad} \sim 25\%$ was obtained without a significant change in stored energy. The radiation enhancement had a slower time constant. The supplemental radiation area of the Kr seeded plasma moved from the HDXs to the core plasma. Highly charged states of Kr ions are considered to be the dominant radiators from the plasma core region.

1. Introduction

Reduction of heat and particle loads to the divertor is one of the important issue to realize a fusion reactor. Divertor detachment is a favorable operation mode for this purpose. To achieve divertor

detachment, it is necessary to reduce the electron temperature (T_e) in the scrape-off-layer (SOL). One of the effective methods for the reduction of T_e is radiation enhancement in the SOL plasma using impurity seeding. In tokamaks, radiation enhancement experiments with impurity seeding have been conducted, and the reduction of T_e in the SOL has been observed [1-7]. In the Large Helical Device (LHD), the structure of the magnetic field line outside the last closed flux surface (LCFS) consists of a stochastic layer, edge surface layers and residual natural islands [8]. In this study, the radiation was enhanced and the heat load of the carbon divertor was reduced by neon (Ne) and krypton (Kr) seeding [9].

2. Experimental setup

The experimental setup is shown in Figure 1. LHD is the largest helical device (R = 3.9 m, a = 0.65 m) with superconducting helical (L/M = 2/10) coil and poloidal coils [10]. In this study, plasma heating was mainly performed using three neutral beam injectors with tangential injection (NBI #1-3), and the magnetic axis position was 3.6 m. Ne and Kr puff were injected from the lower port at 9.5 (9.5-L) and from the lower port at 5.5 (5.5-L) by piezo valves, respectively. The plasma total radiation power (P_{rad}) was measured using a resistive bolometer of a four channel array with a wide angle view installed at the outer port 3 (3-O). Here, P_{rad} was cross calibrated with another resistive bolometers of a 16 channel array installed at the outer port 8 (8-O) by assuming constant radiation from a flux surface both toroidally and poloidally [11]. The line-averaged electron density ($n_{e,bar}$) was obtained from interferometer measurements. Imaging measurement of the plasma radiation was performed using an InfraRed imaging Video Bolometer (IRVB) at the upper port at 6.5 (6.5-U). The emissions from Ne and Kr ions were observed by a SOXMOS spectrometer installed at the outer port at 7 (7-O). Hα and C emissions were measured by an impurity monitor at the outer port at 10 (10-O). Divertor probes have been installed at the inner ports at 2, 4, 6, 7, 8, 9 and 10 (2-I, ... , 10-I).

3. Radiation enhancement using Ne seeding

The typical time evolution of the plasma parameters in a Ne seeded plasma are shown in Figure 2. P_{rad} increased and T_e in the divertor was reduced with the Ne seeding, though the plasma stored energy (W_p), $n_{e,bar}$ and energy confinement parameter only changed slightly. Here, the energy confinement parameter is defined as $W_p/(P_{heating}^{-0.61} n_{e,bar}^{0.54})$ based on the ISS04 scaling [12].

3.1. Operation region of the radiation enhancement in Ne seeded plasmas

Figure 3 indicates the dependence of the radiated power fraction $f_{rad} = P_{rad}/P_{heating}$ on the $n_{e,bar}$ just before the Ne seeding in a number of plasma discharges. P_{rad} was enhanced for all density conditions by the Ne seeding. The power fraction, f_{rad}, is limited by the plasma radiative collapse. The achieved fraction with

Ne seeding is 52% during relatively low density discharges ($n_{e,bar} \sim 1.3 \times 10^{19}$ m^{-3} just before the seeding), while the fraction before the seeding namely in pure hydrogen plasmas is constant around 15% over the range of $n_{e,bar}$ investigated. The fraction is limited up to around 30% in hydrogen plasmas without Ne seeding even for high density plasma ($n_{e,bar} > 1 \times 10^{20}$ m^{-3}) just below the radiative collapse [13]. The radiative collapse is attributed to a radiative thermal instability of light impurities, mainly carbon, in the plasma edge region [13]. The maximum achievable radiated power fraction enhancement using the Ne seeding decreased with increase of density since the enhancement region of the radiation as the composition of C, H, and Ne might be changed due to the reduction of the edge T_e. At high density ($n_{e,bar} > 4 \times 10^{19}$ m^{-3}), f_{rad} is less than 40%. The dependence of the Ne seeding amount on $n_{e,bar}$ before the seeding is shown in Figure 4. It indicates that the injectable amount of the Ne seeding without the radiative collapse decreased with the $n_{e,bar}$. Figure 5 shows the dependence of the power fraction on the normalized energy confinement parameter. Here, $n_{e,bar}$ just before the Ne seeding ranges from 1.0 to 6.8 $\times 10^{19}$ m^{-3} in these discharges, as shown in Figure 3. The ratio of the energy confinement parameter between that during the radiation enhancement and that just before the Ne seeding is plotted as the normalized parameter in Figure 5. The degradation of the confinement during the radiation enhancement remains less than 20% over the operation regime in this study.

3.2. Sustainment of the radiation enhancement using multi-pulse Ne seeding

Multi-pulse Ne seeding has been carried out to sustain the radiation enhancement in a long pulse plasma discharge. The time evolution of the plasma parameters in the discharge with multi-pulse Ne seeding (#121957) and without Ne seeding (#121959) are shown in Figure 6. The first Ne puff was injected for 120 ms at 4.0 s to the plasma of $n_{e,bar} \sim 3.1 \times 10^{19}$ m^{-3}. Then a pulse of 50 ms was injected every 0.5 s. After the first seeding, plasma radiation was enhanced to $f_{rad} \sim 36\%$ and divertor particle flux decreased by 50% in all toroidal sections. Here, the confinement degradation due to the $n_{e,bar}$ increase was less than 8% and it was recovered to the same confinement level of the pure hydrogen plasma before the second seeding. During the short pulses, $f_{rad} \sim 30\%$ was successfully sustained for 3.4 s. Divertor particle flux gradually increased with the decrease of P_{rad}. The plasma was terminated by the end of the NBI heating. Imaging measurement of the plasma radiation using an IRVB [14, 15] was conducted to investigate the radiation profile enhanced by Ne seeding. Figure 7 (a) shows the field of view (FoV) of the IRVB has been installed at an upper port (6.5-U port, in Figure 1) and Figure 7 (b), (c) indicate the radiation profile difference between after Ne seeding (4.3, 6.5 s) and before Ne seeding (3.9 s), respectively. The measurement clearly shows that the radiation enhancement during impurity seeding occurred along the helical divertor X-points (HDXs) and in particular at the inboard side. Since the radiation enhancement is localized in the SOL during the Ne seeding, the degradation of the plasma confinement is relatively small. It is obviously different from the enhancement of the plasma radiation in pure hydrogen plasmas just before the radiative collapse, which does not follow the HDXs and is localized on the inboard side as shown in Figure 7 (d). Figure 8 (a)-(h) show the estimated radiation using EMC3-EIRENE code [16-

18] in the Ne seeding plasma. The plasma radiation is also around the HDXs and the projected image onto the IRVB detector has a structure similar to the experimental data. Figure 9 (a)-(f) show the estimated radiation without the Ne seeding plasma. The radiation structure of the total plasma radiation around the HDXs is not clear compared with the Ne seeding case which is similar to the structure shown in Figure 7 (d). Figure 10 (a) shows the plasma radiation measured with a resistive bolometer array installed at the lower port on the same poloidal section as the IRVB (6.5-L port, in Figure 1). The red line indicates the channel which observes around the magnetic axis without HDXs. Here, the radiation from outside the LCFS is also contained in the core signal due to the line integration. The blue line shows the channel which observed the lower HDX without the plasma core region. The radiation signal of the HDX was higher than the signal from the core plasma although the path length of the HDX channel is shorter than the core plasma channel. Then, the radiation from the edge region seems to be larger than the radiation from the core plasma. Figure 10 (b)-(d) show the signal of Hα and C measured by the impurity monitor and Ne radiation measured by the SOXMOS spectrometer [19]. The time evolution of P_{rad} has similar tendency to C^{3+} and lower charged states of Ne ion (Ne^{3+} and Ne $^{4+}$). Therefore, C and/or Ne are candidates as the dominant radiator in the Ne seeded plasma.

4. Radiation enhancement using Kr seeding

To investigate the plasma radiation characteristics for the optimization of the impurity seeding condition, radiation enhancement has also been carried out using Kr seeding. Figure 11 shows the typical time evolutions of the plasma parameters in a Kr seeded plasma. Kr seeding was conducted from 4.5 s for 1.0 s. Here, a modulated NBI (#4, in Figure 1) of 4 MW was applied in addition to the three tangential NBI of 10 MW for charge-exchange recombination spectroscopy measurements. The radiation enhancement was started from just after the injection. However, the response of the enhancement was slower than the Ne seeded plasma. The power fraction f_{rad} increased to around 25%. Here, the particle flux to the divertor was reduced 20% in some toroidal sections. The confinement degradation was 14%. The radiation enhancement was kept after the Kr seeding. W_p and the confinement degradation around 10% were almost constant while $n_{e,bar}$ gradually increased after the Kr seeding. Figure 12 shows the time evolution of the radiation profile difference between after Kr seeding (5.6, 5.8, 6.0, 6.5 s) and just before Kr seeding (4.4 s). The enhancement of the plasma radiation occurred along the HDXs just after the Kr seeding (a). After that, the enhanced region shifted along the magnetic axis (b-d). This result indicates that the region of the radiation enhancement was moved from the HDXs to the plasma core region. Figure 13 (a) shows the plasma radiation measured with a resistive bolometer array installed at the lower port on the same poloidal section as the IRVB (6.5-L port, in Figure 1). The radiation of the lower HDX decreased from the end of the Kr seeding while the radiation from the core was maintained a slight increase. It is clearly different from the Ne seeded plasma as shown in Figure 10 (a). Figure 13 (c) shows that the time evolutions of normalized intensities of Kr ions measured by the SOXMOS spectrometer. After the Kr seeding (5.5 s), the intensities of Kr^{24+} and Kr^{25+} which emit at around 1 keV decreased

much slower than the intensity of Kr^{7+} . These tendencies of the higher ion stages were similar to the behavior of the plasma radiation from the core region. These results indicate that the highly charged states of Kr ions which radiated at the core plasma are dominant radiators in the Kr seeded plasma.

5. Summary

Impurity seeding experiments were carried out in the LHD using Ne and Kr gases. Plasma radiation enhancement and the reduction of the divertor heat load were observed without significant confinement degradation. 52% radiated power fraction f_{rad} was obtained using Ne puffing in the condition of $n_{e,bar} \sim 1.3 \times 10^{19}$ m^{-3}. Applying the multi-pulse Ne seeding, radiation enhancement was successfully sustained for 3.4 s. From the radiation imaging with an IRVB, the radiation enhancement around the HDXs was observed. In Kr seeded plasma, the response of the radiation enhancement was slower than the Ne seeded plasma. The enhancement area was along the HDXs just after the Kr seeding, after that, the area was moved to the core plasma where the radiation from the higher ion stages are dominant. f_{rad} was 25%, however, the enhanced area was clearly different from the Ne seeded plasma. We plan to carry out experiments in the future combining Ne and Kr to attempt further radiation enhancement. This advanced operation of the impurity seeding condition should be investigated and optimized to realize an 80-90% radiation power fraction for DEMO reactors.

Acknowledgements

The authors thank the LHD technical staff for their excellent support in the LHD experiments. This work is supported by NIFS/NINS (NIFS13ULHH026, NIFS13GGHH001).

References

[1] Maddison G P *et al* 2003 *Nucl. Fusion* **43** 49

[2] Rapp J *et al* 2004 *Nucl. Fusion* **44** 312

[3] Asakura N, Nakano T, Oyama N, Sakamoto T, Matsunaga G and Itami K 2009 *Nucl. Fusion* **49** 115010

[4] Nakano T, Asakura N, Kubo H, the JT-60 team 2013 *J. Nucl. Mater.* **438** S291

[5] Reinke M L, Hughes J W, Loarte A, Brunner D, Hutchinson I H, LaBombard B, Payne J and Terry J L 2011 *J. Nucl. Mater.* **415** S340

[6] Fuchs JC, Bernert M, Eich T, Herrmann A, de Marné P, Reiter B and the ASDEX Upgrade team 2011 *J. Nucl. Mater.* **415** S852

[7] Kallenbach A *et al* 2013 *Plasma Phys. Control. Fusion* **55** 24041

[8] Masuzaki S *et al* 2002 *Nucl. Fusion* **42** 750

[9] Masuzaki S *et al* 2013 *J. Nucl. Mater.* **438** S133

[10] Iiyoshi A *et al* 1999 *Nucl. Fusion* **39** 1245

[11] Peterson B J *et al* 2010 *Fusion Sci. Technol.* **58** 412

[12] Yamada H *et al* 2005 *Nucl. Fusion* **45** 1684

[13] Peterson B J *et al* 2006 *Plasma Fus. Res.* **1** 045

[14] Peterson B J *et al* 2011 *J. Nucl. Mater.* **415** S1147

[15] Mukai K, Peterson B J, Pandya S N, Sano R and Itomi M 2014 *Plasma Fusion Res.* **9** 3402037

[16] Feng Y *et al* 2004 *Contrib. Plasma Phys.* **44** 57

[17] Reiter D *et al* 2005 *Fusion Sci. Technol*. **47** 172

[18] Kobayashi M 2010 *Fusion Sci. Technol.* **58** 220

[19] Schwob J L *et al* 1987 *Rev. Sci. Instrum.* **58** 1601

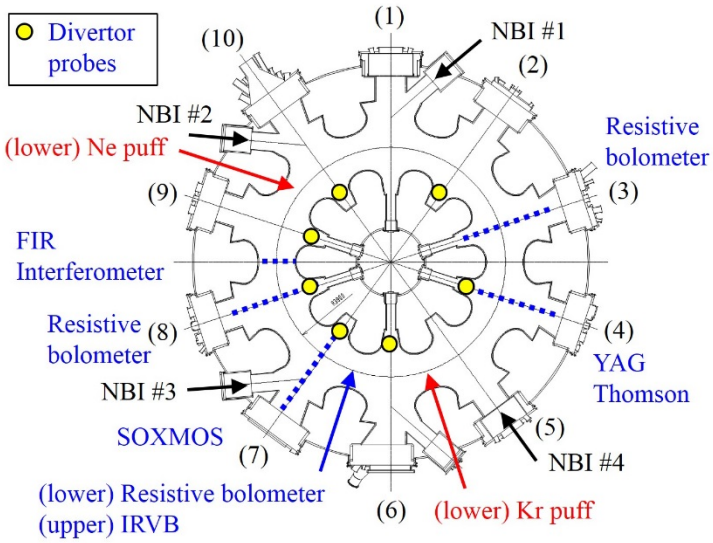

Figure 1. Experimental setup in LHD. Ne and Kr puff were injected from the bottom ports at 9.5 and 5.5 ports, respectively.

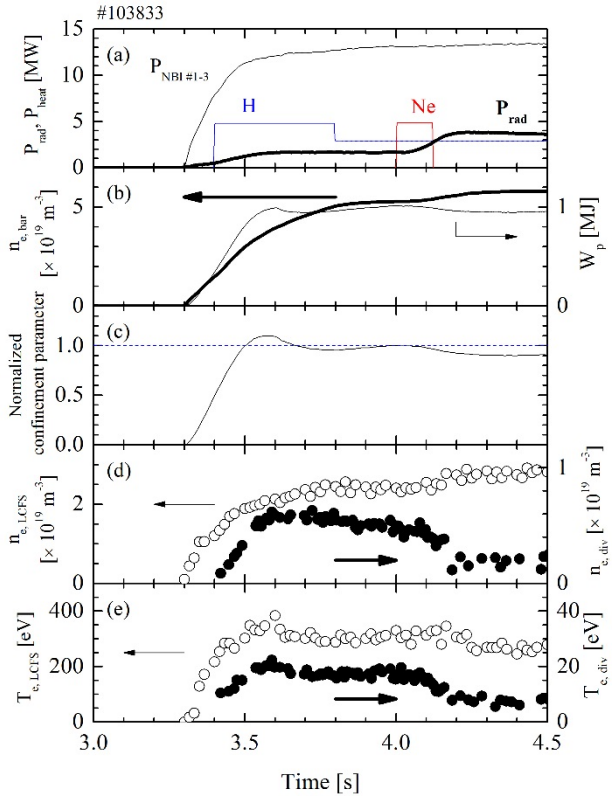

Figure 2. Typical time evolutions (#103833) of (a) heating and radiation power, Ne and H seeding, (b) line averaged density and plasma stored energy, (c) energy confinement parameter normalized at $t = 4.0$ s, (d), (e) electron density and temperature at LCFS and at the 6-I divertor probe.

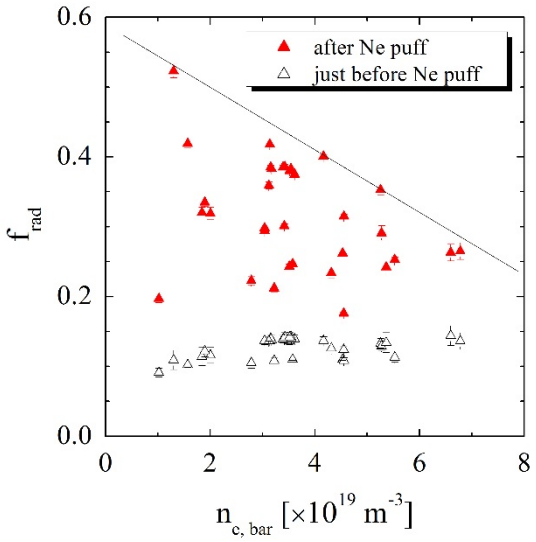

Figure 3. The radiated power fraction just before/after detachment versus line averaged electron density in the Ne seeding discharges. Red filled triangles and black triangles indicate the maximum f_{rad} after the Ne seeding and the f_{rad} just before the Ne seeding. The line is an eye guide.

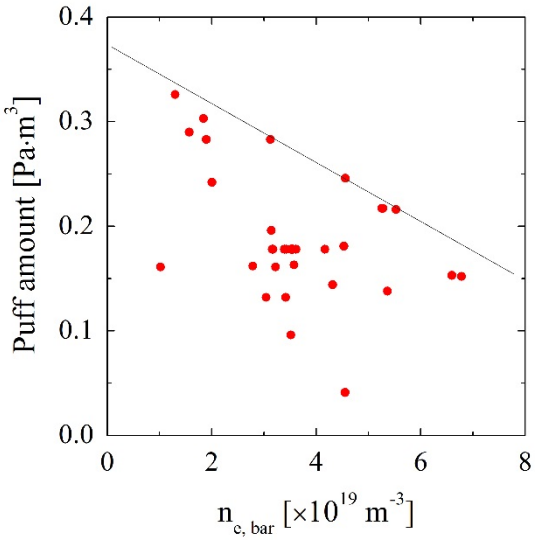

Figure 4. Amount of the Ne seeding versus line averaged electron density. The line is an eye guide.

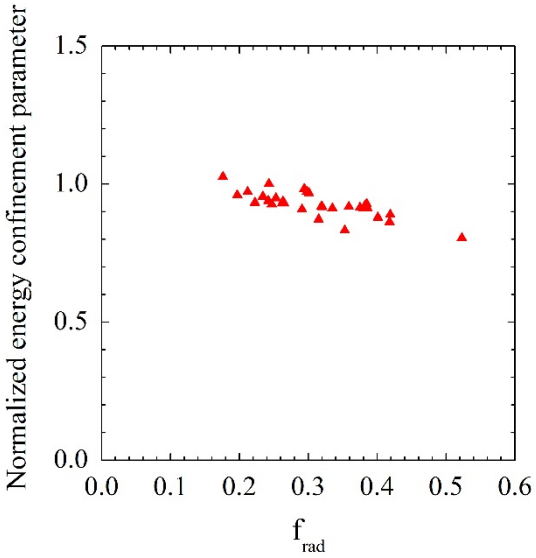

Figure 5. Energy confinement parameter in detached plasmas vs. the radiated power fraction after detachment in the Ne seeding discharges. The confinement degradation was suppressed to less than 20%.

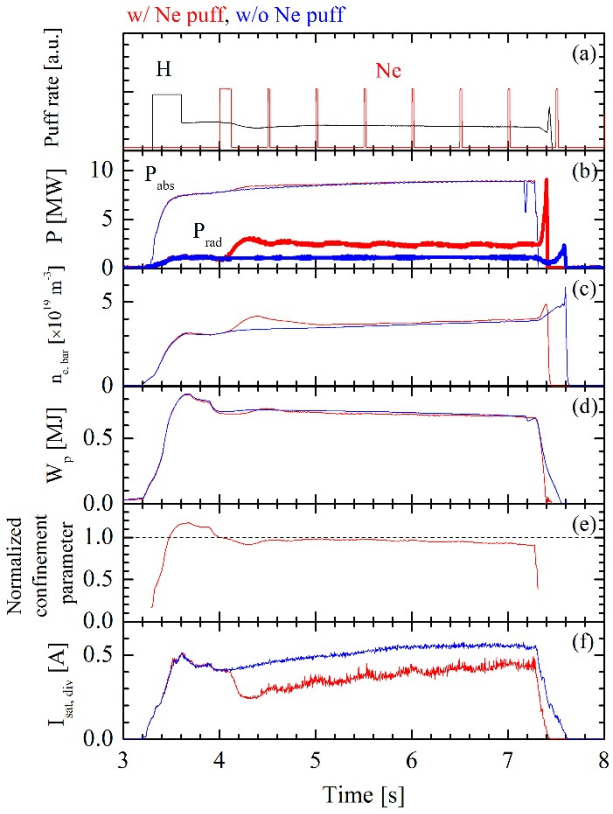

Figure 6. Time evolutions in the plasma discharge with multi-pulse Ne seeding (#121957, red) and without Ne seeding (#121959, blue). (a) Ne and H seeding (H was injected in both cases), (b) heating and radiation power, (c) line averaged density, (d) plasma stored energy, (e) energy confinement parameter normalized at t = 4.0 s, (f) ion saturation current at the 6-I divertor probe, $I_{sat,\,div}$.

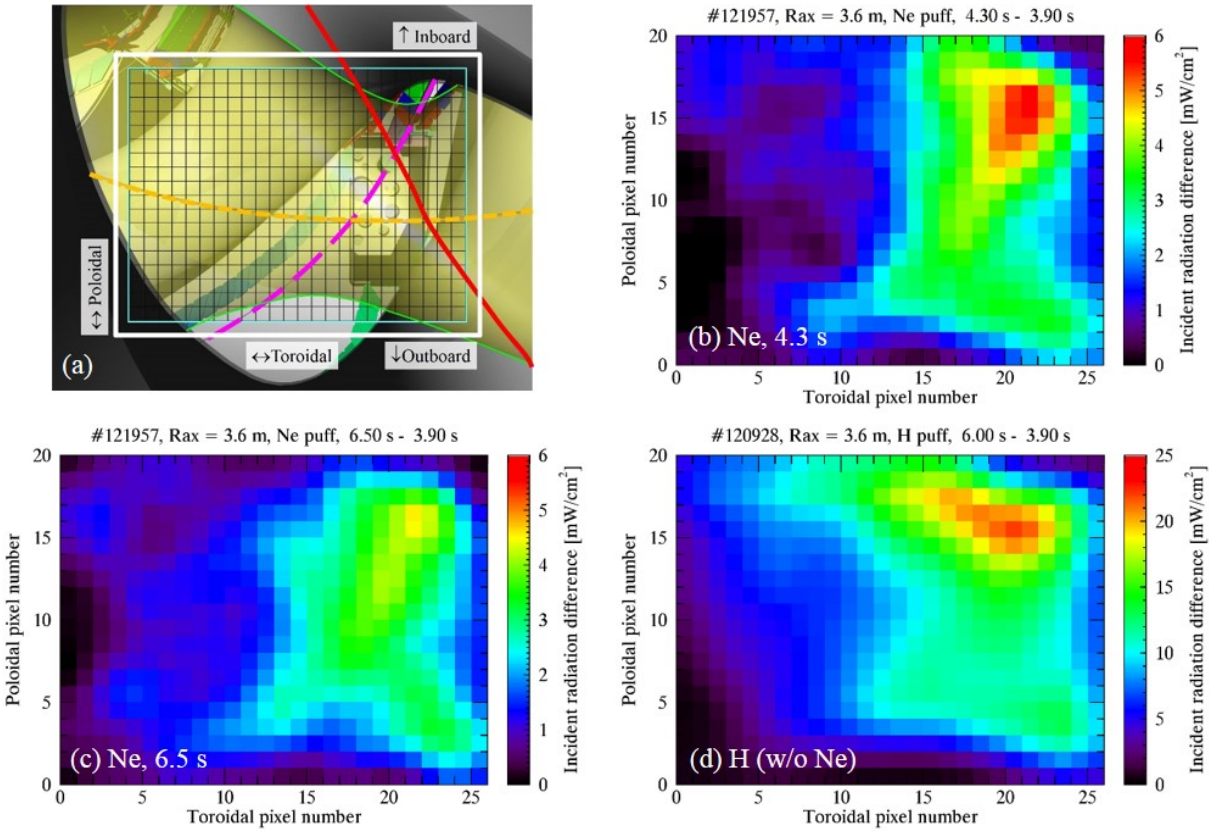

Figure 7. (a) CAD image of IRVB FoV from an upper port (white rectangular). Solid (red) and dashed (magenta) lines indicate upper and lower HDXs, respectively. Short dashed (orange) line shows magnetic axis. Thin (green) lines indicate LCFS. **(b), (c)** Observed enhancement of the radiation between after and before Ne seeding (#121957) at t = 4.3 s and 6.5 s. **(d)** Observed enhancement in pure H plasma just before the radiation collapse (#120928).

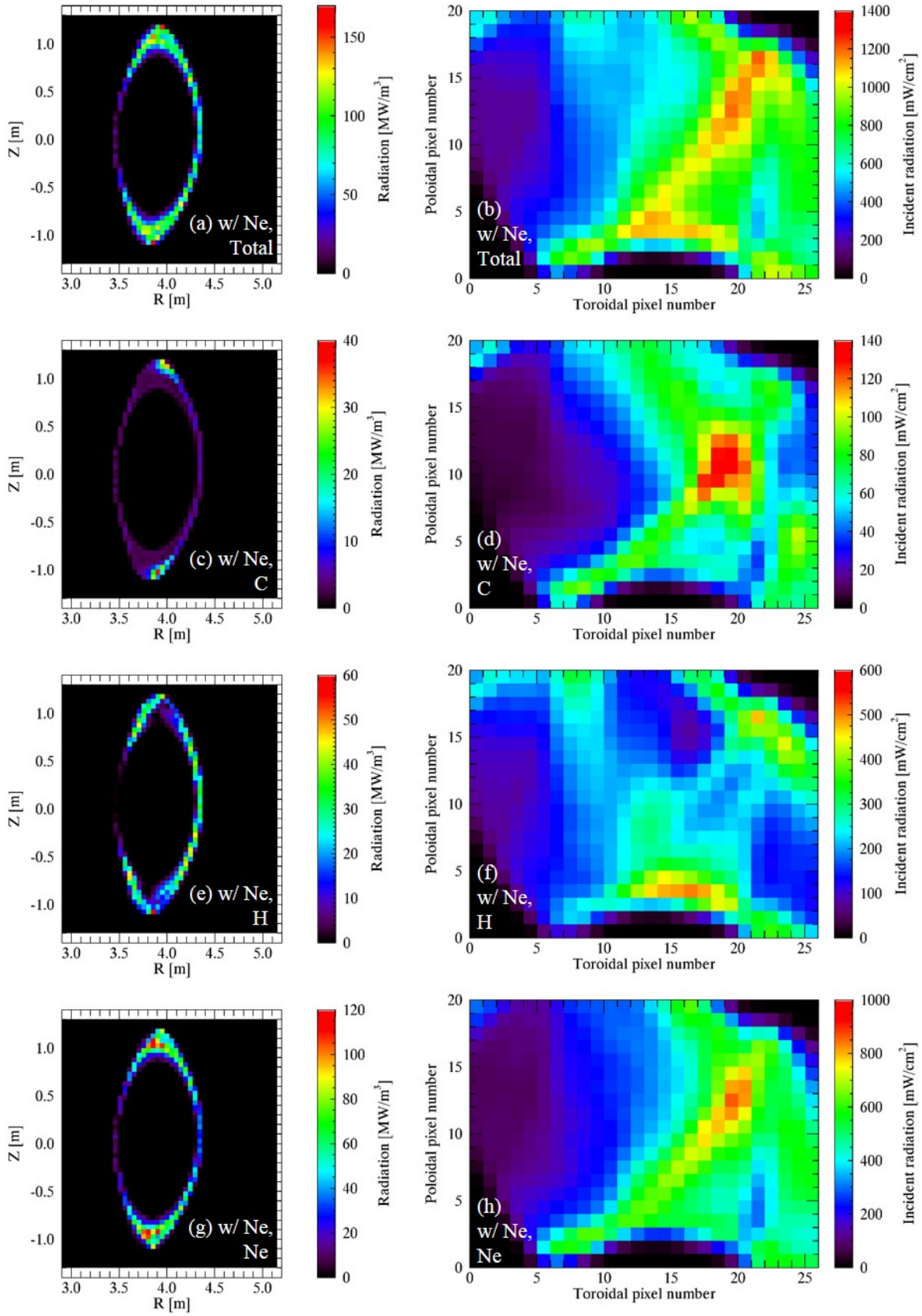
(a) w/ Ne, Total
(b) w/ Ne, Total
(c) w/ Ne, C
(d) w/ Ne, C
(e) w/ Ne, H
(f) w/ Ne, H
(g) w/ Ne, Ne
(h) w/ Ne, Ne
Z [m]
R [m]
Radiation [MW/m^3]
Poloidal pixel number
Toroidal pixel number
Incident radiation [mW/cm^2]

Figure 8. Radiation with the Ne seeding plasma estimated by EMC3-EIRENE code **(a)**, **(b)** of composition of C, H, and Ne, **(c)**, **(d)** of C, **(e)**, **(f)** of H, and **(g)**, **(h)** of Ne in the poloidal cross section of the IRVB and as the projection image onto the IRVB detector, respectively.

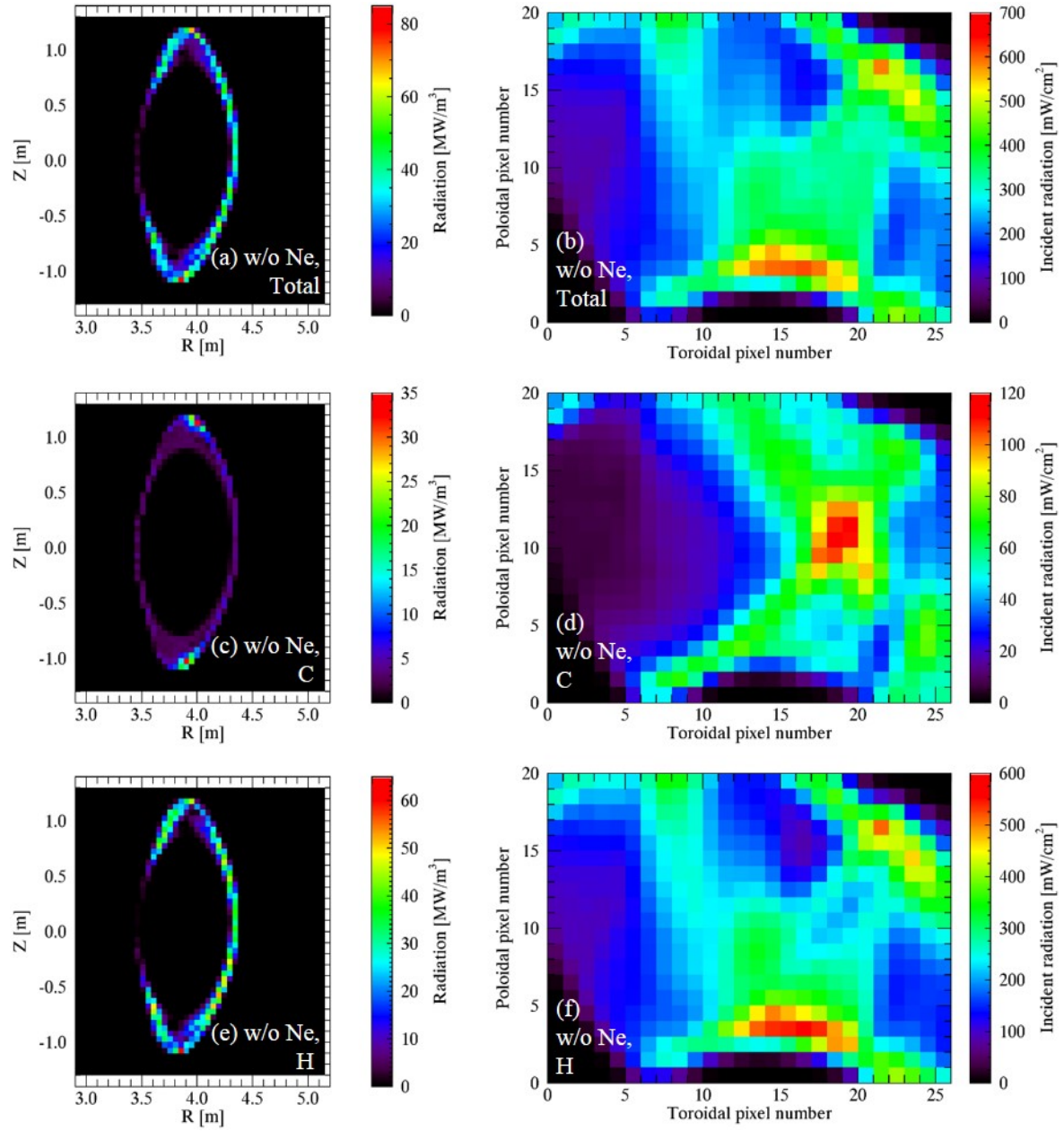

Figure 9. Radiation without the Ne seeding plasma estimated by EMC3-EIRENE code **(a)**, **(b)** of composition of C and H, **(c)**, **(d)** of C, and **(e)**, **(f)** of H in the poloidal cross section of the IRVB and as the projection image onto the IRVB detector, respectively.

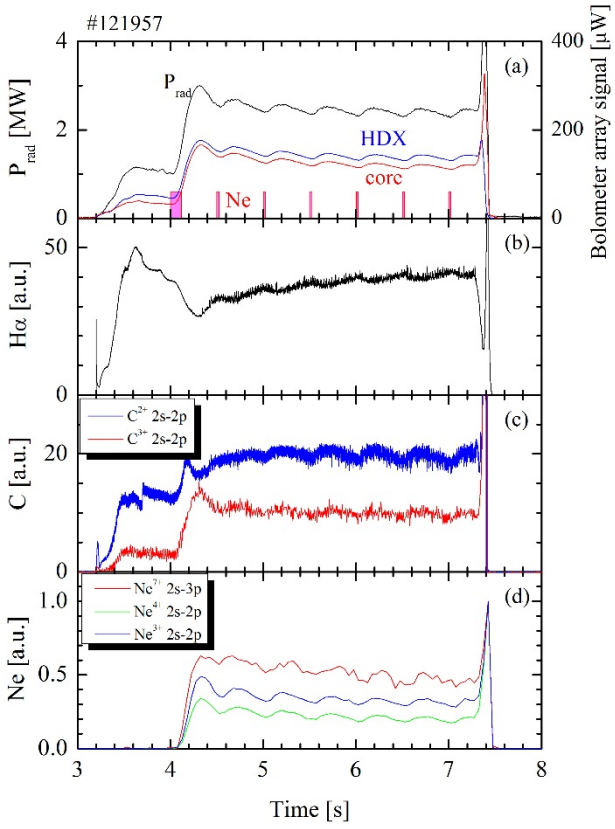

Figure 10. Time evolutions of (a) P_{rad} and resistive bolometer array signals (injected radiation power to the foil of 1.5×4 mm) with the sight lines of the core plasma (red) and lower HDX (blue), (b) Hα, (c) C radiations and (d) Ne radiations in the Ne seeded plasma.

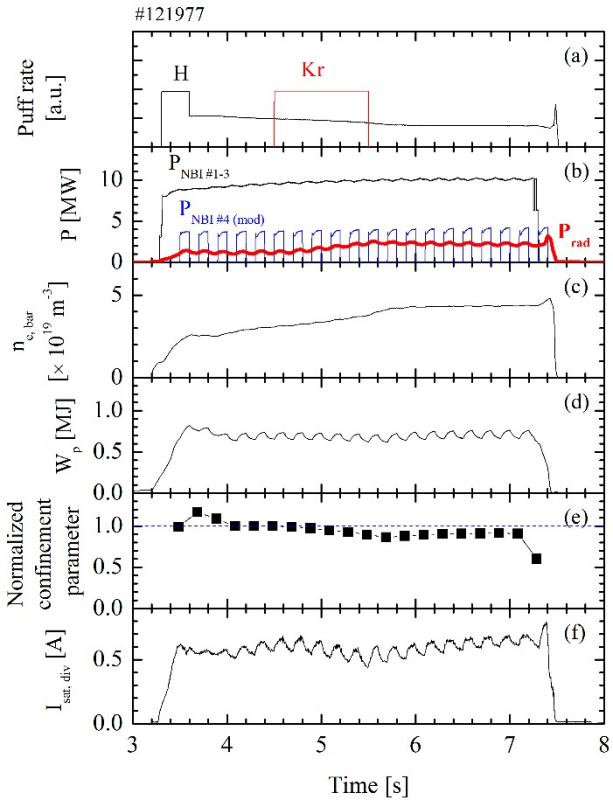

Figure 11. Typical time evolutions of the Kr seeded plasma (#121977). **(a)** Kr and H seeding, (b) heating and radiation power, **(c)** $n_{e,bar}$, **(d)** W_p, **(e)** normalized energy confinement parameter normalized at t = 4.5 s, and **(f)** $I_{sat,div}$ at the 2-I divertor probe.

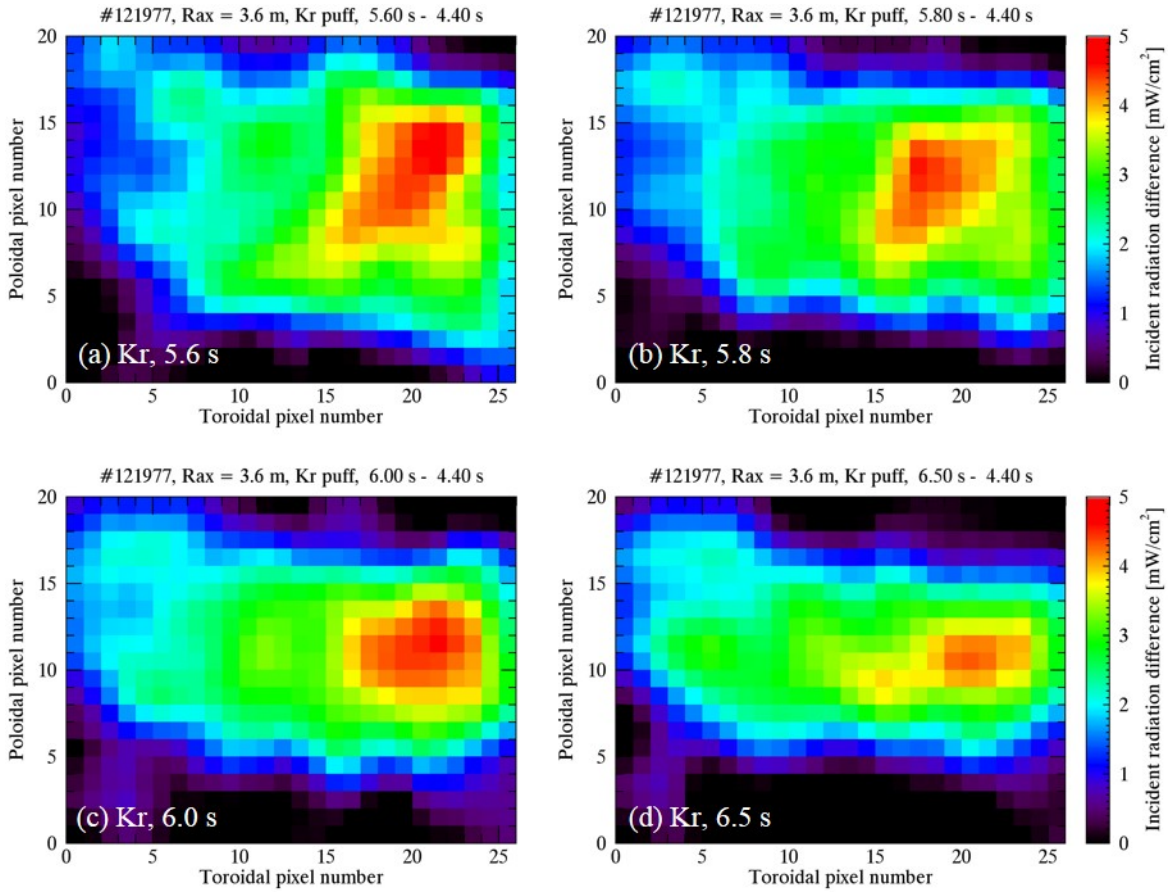

Figure 12. Observed enhancement of the radiation between after and before Kr seeding (#121977). The supplemental radiation area was along the HDXs just after the Kr seeding **(a)**. However, it was gradually shifted to along the magnetic axis **(b)-(d)**.

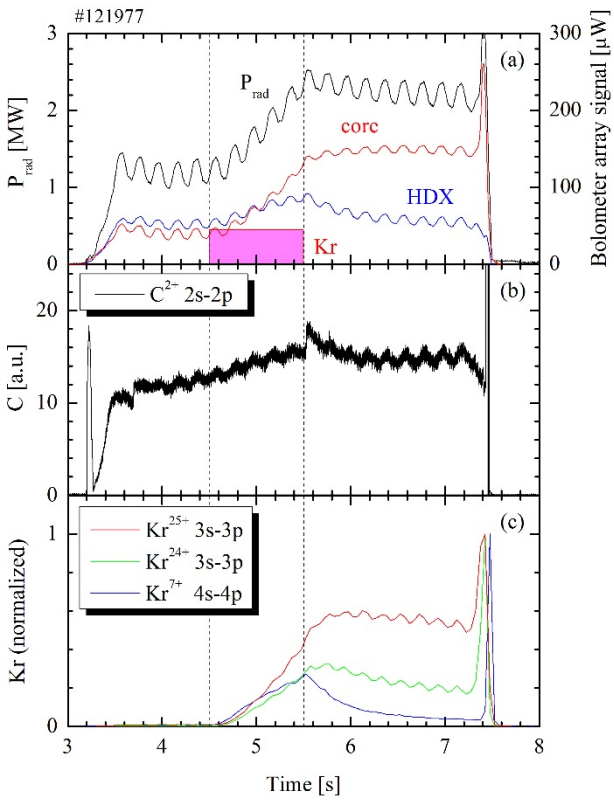

Figure 13. Time evolutions of (a) P_{rad} and resistive bolometer array signals with the sight lines of the core plasma (red) and lower HDX (blue), (b) C and (c) Kr radiations in the Kr seeded plasma.